



Original

## Transistor characteristics of zinc oxide active layers at various zinc acetate dihydrate solution concentrations of zinc oxide thin-film

H.C. You

*Department of Electronic Engineering, National Chin-Yi University of Technology, Taiwan*

Received 19 April 2014; accepted 18 August 2014

### Abstract

This paper presents a technique involving a sol-gel deposition method applied to the deposition of zinc oxide thin film for a transistor as a semiconductor layer. This method was used for manufacturing the essential thin films of II-VI semiconductors. Zinc oxide (ZnO) bottom-gate (BG) thin-film transistors (TFTs) have been successfully fabricated at low temperatures. We investigated the electrical characteristics of ZnO thin-film transistors at various concentrations of ZnO solution: 0.02 M, 0.03 M, 0.04 M, and 0.05 M. All of the ZnO films exhibited a hexagonal wurtzite polycrystalline structure with (002) preferred orientation. Atomic force microscopy (AFM) revealed the formation of grains or clusters as a result of the accumulation of nanoparticles, and the grain size increased with increasing solution concentration. The coated ZnO films were employed as the active channel layer in thin-film transistors, and the impact of the solution concentration on the device performance was examined. As the solution concentration was increased, the field-effect mobility increased from  $1 \times 10^{-4} \text{ cm}^2/\text{V}\cdot\text{s}$  to  $1.2 \times 10^{-1} \text{ cm}^2/\text{V}\cdot\text{s}$ , the threshold voltage increased from 4.8 V to 11.1 V, and the  $I_{\text{on}}/I_{\text{off}}$  ratio increased from  $10^4$  to  $10^6$ . The on-off ratio ( $I_{\text{on}}/I_{\text{off}}$ ) was found to be  $10^6$ . The 0.05 M ZnO solution performed optimally.

All Rights Reserved © 2015 Universidad Nacional Autónoma de México, Centro de Ciencias Aplicadas y Desarrollo Tecnológico. This is an open access item distributed under the Creative Commons CC License BY-NC-ND 4.0.

**Keywords:** ZnO; Zinc acetate dihydrate solution; Thin-film transistor; Concentration

### 1. Introduction

Matrices of thin-film transistors (TFTs) in next-generation displays not only require semiconductors with high performance, but also require them to feature high optical transparency, and low-temperature and solution processability (Ameer 2012; Bermudez-Reyes et al., 2012; Grundmann et al., 2010). To date, hydrogenated amorphous silicon (a-Si:H)-based TFTs have been widely used as pixel switches in displays (Spear & Le Comber, 1993). However, amorphous silicon with deposition requires a high-cost vacuum process. More important, the poor transparency of silicon makes it unsuitable for transparent applications, and transparency is a key criterion for future display technology. Consequently, metal oxide semiconductors, such as In, Ga or Zn oxides (Park et al., 2012), have gained considerable interest as alternatives for amorphous silicon.

Generally, metal oxide thin films have been used as electrodes in flat panel displays such as  $\text{In}_2\text{O}_3$ ,  $\text{SnO}_2$ , and ZnO. Indium is currently the most commonly used material, but it is costly and toxic. Compared to the high price of In, Zn is inexpensive. In the recent years, ZnO thin films have been consid-

ered favorable candidates to be metal oxide materials because of their efficient visible transmittance, optimal conductivity, and low-cost fabrication (Cho et al., 2010).

Zinc oxide (ZnO) is a II-VI *n*-type compound semiconductor that possesses several favorable characteristics, including a wide energy bandgap (3.3 eV) (Chu et al., 2012; Lee et al., 2003; You & Lin 2012), large free exciton binding energy (60 mV), wide range resistivity ( $10^{-4}$  to  $10^{12} \Omega \text{ cm}$ ), high carrier mobility, high transparency at room temperature, and excellent photoelectric, piezoelectric, and thermoelectric properties (Tsay et al., 2010). ZnO has a natural *n*-type conduction because of a large number of native defects, such as oxygen vacancies and zinc interstitials. ZnO crystallizes in a hexagonal wurtzite structure exhibiting non-central symmetry; therefore, it demonstrates piezoelectricity (Anand et al., 2010). The conduction band of ZnO is primarily composed of large, metal-based 4s orbitals that expand spatially into isotropic shapes, thus enabling the direct overlap between neighboring metal orbitals. The unique properties of the conduction band have led to recent interest in using ZnO as a channel material for TFTs, and as a replacement for conventional Si-based materials and organic semiconductors (Kim et al., 2009). ZnO-based TFTs have received a considerable amount of attention for the following practical applications: active matrix organic light emitting di-

*E-mail address:* [heyou@ncut.edu.tw](mailto:heyou@ncut.edu.tw) (H.C. You).

ode (LED) displays; radio frequency identification tags; low-end smart cards; and sensing devices on polymer substrates by using organic field-effect transistors.

ZnO-based films are prepared using various deposition techniques, such as pulsed laser deposition, sputtering, atomic layer deposition, and chemical vapor deposition (CVD), all of which usually suffer from the following problems: high cost, low throughput complex operating conditions, and high energy consumption. By contrast, solution-based deposition processes, such as the sol-gel process, chemical bath deposition, and the aqueous solution growth method, have offered comparatively simple, low-cost, and large area thin-film deposition techniques (Cheng et al., 2011). The sol-gel method not only enables easy fabrication of a large area thin film at a low cost, but also easily controls the film composition and uniformity of thickness (Bahadur et al., 2007; Bari et al., 2009; Gayen et al., 2011).

The primary aim of this work is to investigate the fabrication of ZnO films in a zinc acetate sol-gel solution under electroless conditions, as well as its impact on the electronic properties of TFTs (Cheng et al., 2007; Srinivasan et al., 2008). A series of ZnO films are formed at various concentrations of zinc acetate

dihydrate solution (Hoffman et al., 2003; Muthukumar et al., 2001; Pearton et al., 2005). The film nanostructure is investigated using a wide range of characterization techniques, such as atomic force microscopy (AFM) and X-ray diffraction (XRD). In addition, the saturation mobility ( $\mu_{\text{sat}}$ ), on/off current ratio, and threshold voltage of the ultra-thin *n*-type ZnO transistor, with respect to long-term reliability, was carefully investigated based on bottom-gate and top-contact transistor architecture (Hirao et al., 2008).

## 2. Experimental details

A fabrication process flow chart of the ZnO-TFTs is shown in Figure 1A and B. The channel width (*W*) and length (*L*) of the ZnO TFTs were 70 and 2000  $\mu\text{m}$ , respectively. Bottom-gate TFTs with the ZnO channel, which were formed using the sol-gel method at atmospheric pressure. A 100-nm-thick wet oxide layer was deposited using a horizontal furnace to form the gate dielectric on the silicon substrate.

As shown in Figure 2, the ZnO solution sample formed channels of TFTs, and ZnO solutions of 0.02 M, 0.03 M, 0.04 M, 0.05 M, and 0.06 M were prepared using the sol-gel method. The ZnO sol was prepared in ethanol by blending zinc acetate dihydrate [ $\text{Zn}(\text{CH}_3\text{COO})_2 \cdot 2\text{H}_2\text{O}$ ], stirred at 50  $^\circ\text{C}$  for 30 min, and sonicated for 30 min to attain a homogeneous solution. Under the same conditions for the solution, 0.05 M was considered the maximum solubility, because the solution concentration at 0.06 M produced a precipitate. The bottom picture of Figure 2 presents the transparency of test samples. It proved that the zinc oxide thin films are transparent (Lee et al., 1996; Lim et al., 2008; Rendón et al., 2012; Vázquez-Cerón et al., 2007; Wu et

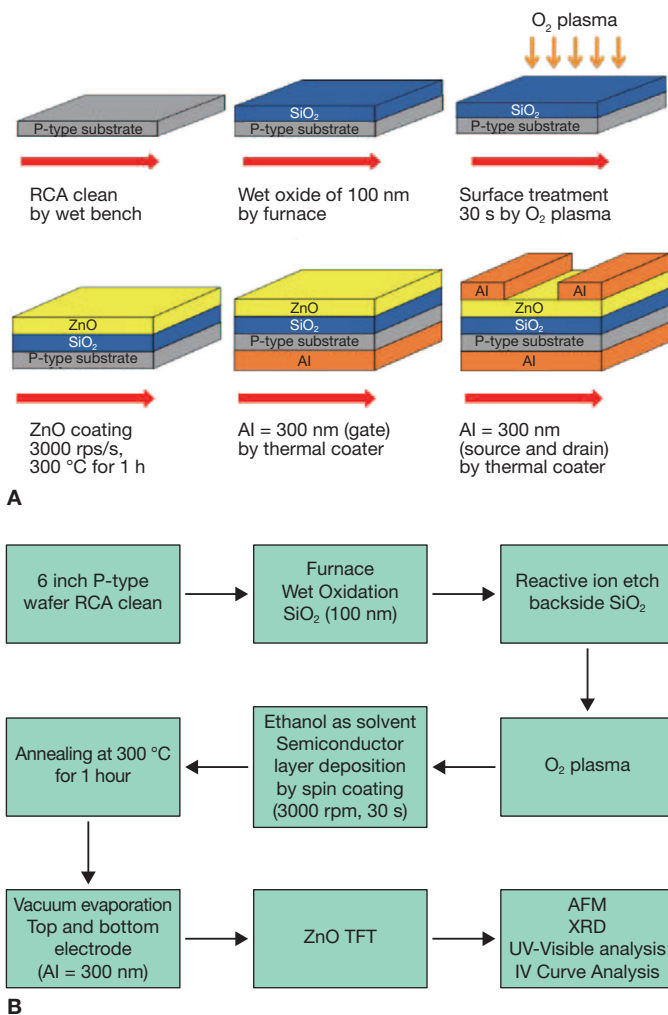


Fig. 1. A: the cross section views and process parameters of ZnO TFT under process sequence flows. B: the process details of ZnO TFT under process sequence flows.

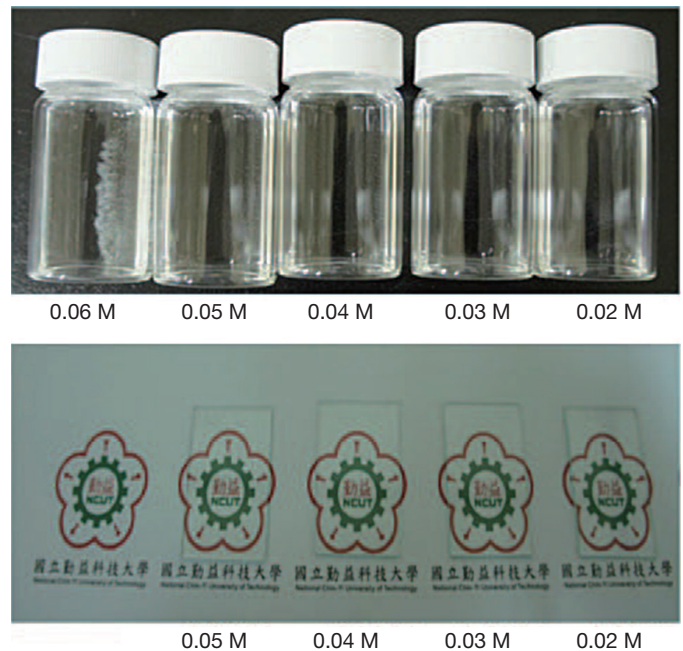


Fig. 2. Solution samples of ZnO concentration from 0.06 M to 0.02 M, spin coating on the glass are transparent.

al., 1998). To enhance compatibility at the interface between the  $\text{SiO}_2$  dielectric and the ZnO active layer, the  $\text{SiO}_2$  dielectric was  $\text{O}_2$ -plasma-treated for 30 s. When  $\text{SiO}_2$  was treated with  $\text{O}_2$  plasma, the chains on the surface were broken, and polar and hydrophilic functional groups such as  $-\text{OH}$  and  $-\text{COOH}$  were introduced, which resulted in an increase of the surface energy (Chang et al., 2007). At the next stage, the ZnO solutions were sequentially spin-coated on the substrate to form a channel, and then followed by soft baking at  $250^\circ\text{C}$  for 5 min, and hard baking at  $300^\circ\text{C}$  for 1 h (ZnO) in ambient air (Lee et al., 2010). After the active layer formed, thermal evaporation was performed to fabricate the source, drain and gate. The 300-nm-thick source and drain were defined using a shadow Al-plated mask and 300-nm-thick gate electrode. After the TFT fabrication, a semiconductor parameter analyzer (4156C, Agilent Technologies), integrated with a probe station, was used to measure the I-V characteristics.

### 3. Results and discussion

The surface properties of ZnO films on Si/ $\text{SiO}_2$  substrates were investigated using atomic force microscopy. The recorded phase and topography images are depicted in Figure 3. Images were acquired in contact mode, and the collected scan area was

$1\ \mu\text{m} \times 1\ \mu\text{m}$ . Here, the root mean square (RMS) roughness was 1.304 nm at the 0.02 M concentration channel layer, 1.887 nm at the 0.03 M concentration channel layer, 1.903 nm at the 0.04 M concentration channel layer, and 4.392 nm at the 0.05 M concentration channel layer. Thus, grain size increases with increasing concentration. This effect could be attributed to the accumulation of nanoparticles forming grains or clusters. By increasing the solution concentration, these clusters grow larger, resulting in film that is more compact. Note that the grain size is not proportional to the increasing concentration. Despite this, however, the 0.05 M solution has the largest grain.

The room-temperature spin-coated films of ZnO, deposited on silicon substrates, were also investigated using XRD, operating in Bragg-Brentano configuration. For these specific measurements, data acquisition was performed using a  $0.08^\circ$  step width. Peak positions were determined by fitting the diffraction pattern data to a pseudo-Voigt function. Basal spacings that characterize these layered compounds were obtained using the Bragg equation. Figure 4 shows the XRD diffraction patterns of ZnO films deposited at 0.03 M, 0.04 M, and 0.05 M, revealing a crystalline structure with a wurtzite (hexagonal) phase and a (002) preferred orientation (along the c-axis). In addition to the ZnO diffraction peaks, the patterns in Figure 2 display an additional peak centered at  $2\theta \approx 60^\circ$ , which is related to the silicon substrate.

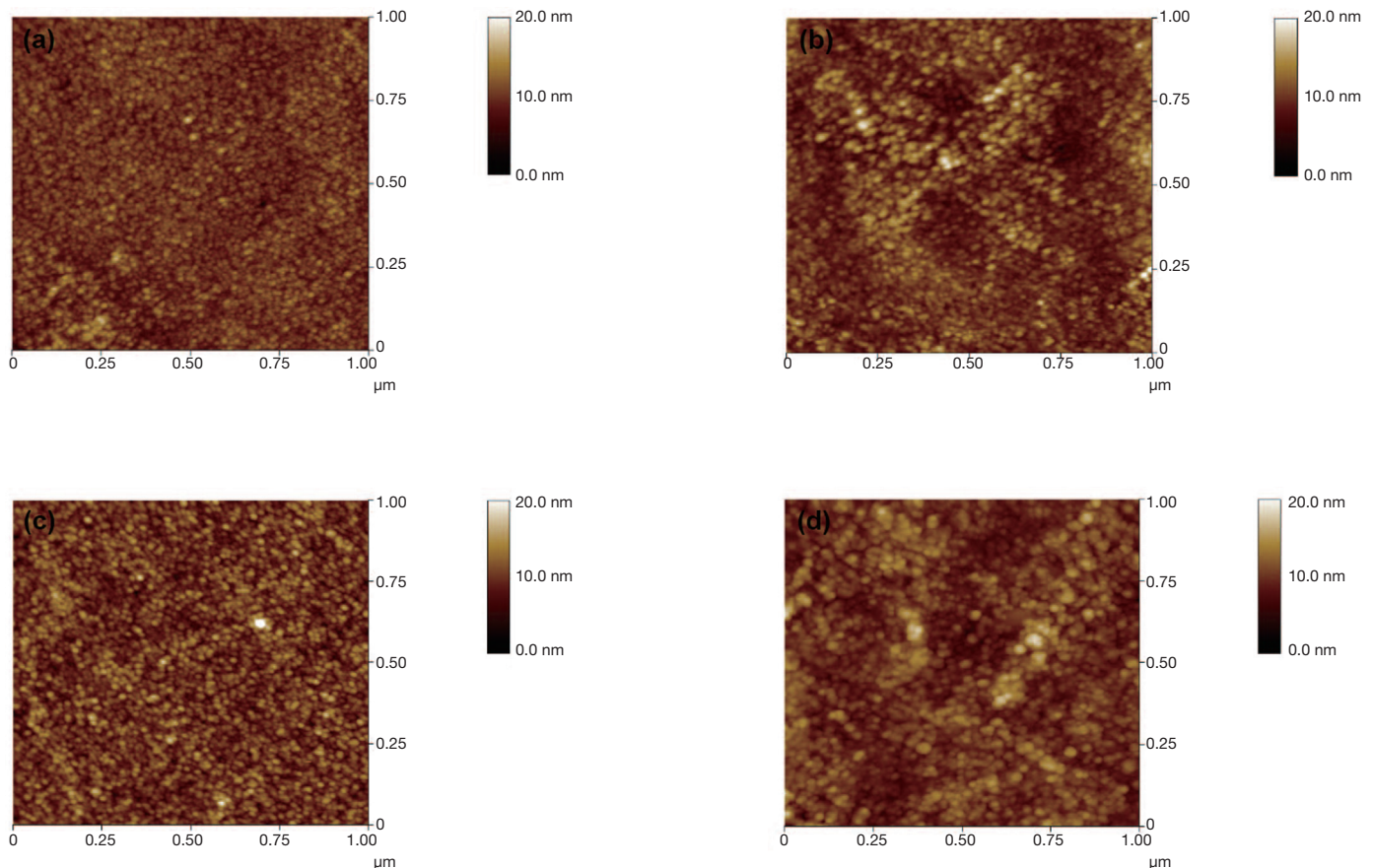


Fig. 3. AFM images of the surface morphology of the ZnO film deposited at room temperature. A: 0.02 M. B: 0.03 M. C: 0.04 M. D: 0.05 M.

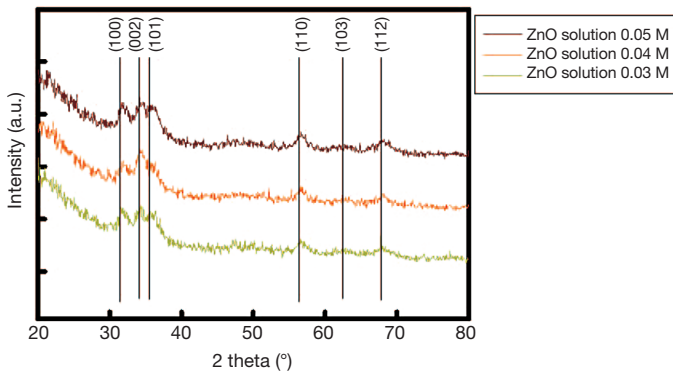


Fig. 4. XRD diffractograms for ZnO films on Si substrates prepared at 0.03 M (A), 0.04 M (B) and 0.05 M (C). Black lines indicate the position of the diffraction peaks of ZnO.

The UV-Vis transmission spectra of ZnO films grown on glass are shown in Figure 5. The spectra clearly demonstrate that the optical transmittance near the band edge of the coated films increases with the increasing solution concentration. The average optical transmission of the entire TFT structure in the visible range of the spectrum is approximately 86%, whereas the transmission at 550 nm (maximum sensitivity for human eyes) is 89%. The average optical transmission of the glass substrate in the visible part of the spectrum is approximately 90%.

In addition, the electrical properties of the ZnO films grown using spin coating at various solution concentrations were investigated using carefully optimized bottom-gate, top-contact transistor architectures, with aluminum (Al) as the source, drain, and gate electrodes. Figure 6 shows the transfer curves of drain current  $I_D$  versus gate voltage  $V_G$ , at a fixed drain voltage  $V_D$  of 5 V for TFTs. The devices were measured at solution concentrations 0.02 M, 0.03 M, 0.04 M, and 0.05 M. Based on the  $I_D$  versus  $V_G$  curves it was concluded that TFTs operate in enhancement mode, because positive gate voltages are required to activate the devices. These graphs also show the variation of drain current in the off-state  $I_{off}$  as a function of power. As shown in Figure 6, at the concentration 0.02 M, and gate volt-

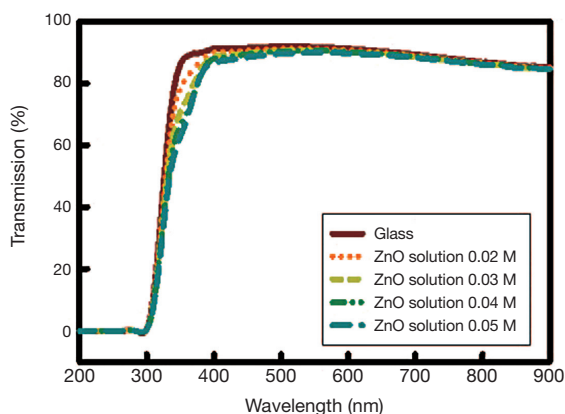


Fig. 5. Optical transmission (%) spectra of ZnO films coated onto Si substrates with ZnO solution concentration in the range of 0.02 M to 0.05 M.

age ( $V_{GS}$ ), no modulation effect on the drain current ( $I_{DS}$ ) was observed. At the concentration 0.05 M,  $I_{DS}$  can be effectively modulated using  $V_{GS}$ . The on-off ratio ( $I_{on}/I_{off}$ ) was found to be  $10^6$ . The lower  $I_{on}$  of the TFT with 0.03 M and 0.04 M could be attributed to the poor contact of the ZnO grain, because the lower ZnO solution cannot take the shape of a dense ZnO grain.

Figure 7 shows  $I_D$ - $V_D$  curves of ZnO-based TFTs for different various solution concentrations. For these measurements, devices with a channel length of  $L = 2000 \mu\text{m}$ , and channel width of  $W = 70 \mu\text{m}$  were used. The gate to source voltage ( $V_G$ ) was varied from 0 to 40 V in steps increments of 5 V. The curves show the typical behavior of a TFT device with an  $n$ -type semiconductor active channel layer (a positive gate to source voltage induces electron channel accumulation). Pinch-off is observed in the electrical response of the four devices processed with at different various concentrations. The main difference observed is the level of current saturation, which goes increases from  $1.52 \times 10^{-5}$  A, for the device processed at 0.02 M, to about approximately  $3.14 \times 10^{-5}$  A, for the one device processed at 0.05 M (at  $V_G = 0$  V in both cases).

In Table 1, the mobility was observed to increase with solution concentration, with the highest value at  $0.12 \text{ cm}^2/\text{V}\cdot\text{s}$ . The lowest  $\mu_{FE} 1 \times 10^{-4} \text{ cm}^2/\text{V}\cdot\text{s}$  was found in TFTs with ZnO channel layer coating 0.02 M solution. This result could be associated with mobility degradation caused by high grain-boundary density in the ZnO channel, as shown in AFM images (Fig. 3). As the grain size decreases,  $V_{th}$  increases. This occurs because, for a given channel dimension, the number of grain boundaries increases and the carriers will therefore have to overcome additional potential barriers. When the concentration of the ZnO solution is 0.05 M, the on current is  $5.11 \times 10^{-5}$ . At on state, the channel mobility is  $0.12 \text{ cm}^2/\text{V}\cdot\text{s}$ , and the threshold voltage is 11.1 V. Thus, the characteristic of TFT is the most stable for the ZnO solution concentration of 0.05 M.

The drain current saturation characteristic for TFT operated in saturation regime is shown in Equation (1).

$$I_{D,sat} = \frac{mW\mu_{eff}C_{ox}}{L}(V_{GS} - V_{th})^2 \quad (1)$$

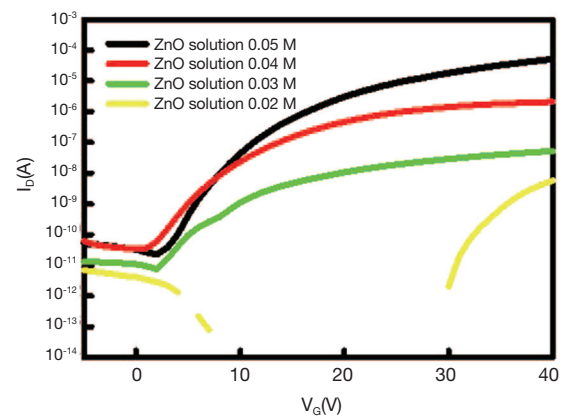


Fig. 6. The characteristics of drain-source current ( $I_{DS}$ ) vs. gate-source voltage ( $V_{GS}$ ) of the ZnO-TFT with respect to the concentrations of ZnO solution: 0.02 M, 0.03 M, 0.04 M, and 0.05M.

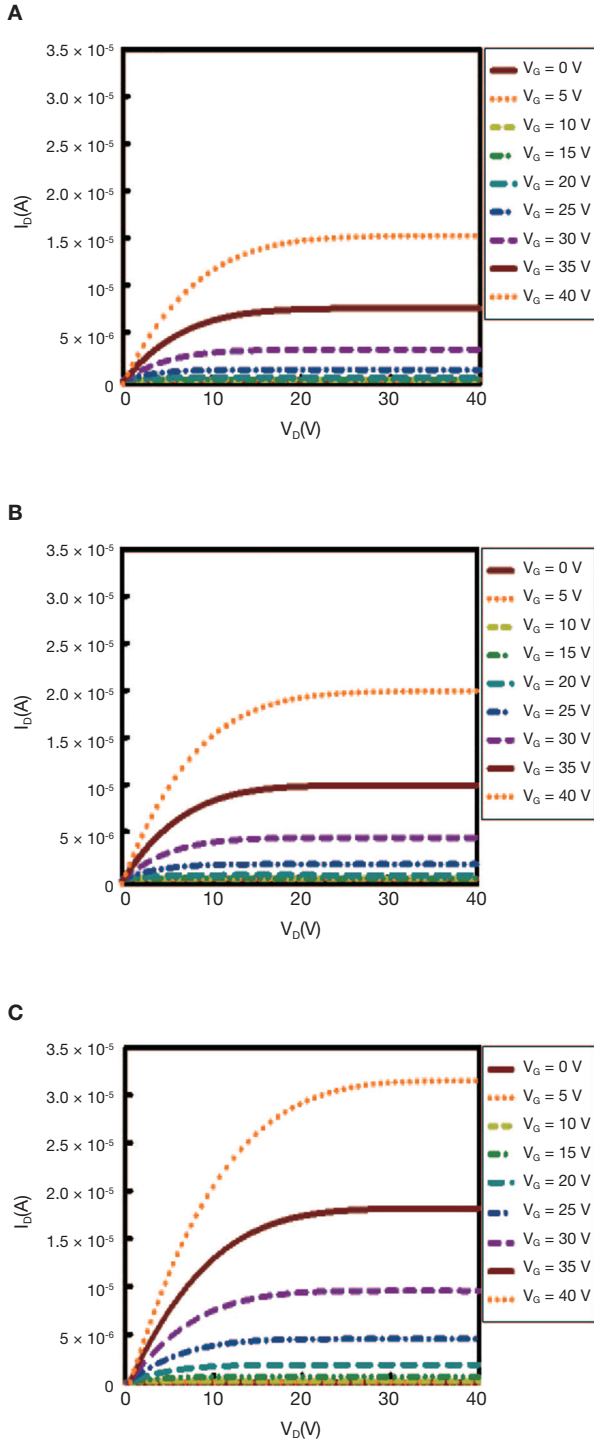


Fig. 7. The characteristics of drain-source current ( $I_D$ ) vs. drain-source voltage ( $V_D$ ) of the ZnO-TFT with respect to the concentration of ZnO solution. A: 0.03 M. B: 0.04 M. C: 0.05 M.

where  $m$  is doping density,  $W$  is channel width,  $L$  is channel length,  $C_{OX}$  is the gate oxide capacitance per unit area, and  $\mu_{eff}$  is effective mobility. Threshold voltage is determined by plotting  $I_D^{1/2}$  versus  $V_G$ , and extrapolating the point of maximum slope (Anand et al., 2010).

The field effect mobility ( $\mu_{FE}$ ) is determined from the transconductance ( $g_m$ ) expressed as:

Table 1

Electrical characteristics of the ZnO-TFT with different concentrations of ZnO solution.

	0.05 M	0.04 M	0.03 M
On current (A)	$5.11 \times 10^{-5}$	$2.08 \times 10^{-6}$	$5.22 \times 10^{-8}$
Off current (A)	$2.31 \times 10^{-11}$	$3.54 \times 10^{-11}$	$1.35 \times 10^{-11}$
On-off ratio	$10^6$	$10^5$	$10^4$
$V_{th}$ (V)	11.1	13.5	4.8
$\mu_{FE}$ ( $cm^2/V\cdot s$ )	0.12	0.006	$1 \times 10^{-4}$

$$g_m = \left. \frac{\partial I_D}{\partial V_{GS}} \right|_{V_{DS}} = \text{constant} \quad (2)$$

When  $V_{GS} > V_{th}$ , the drain current ( $I_D$ ) defined as

$$I_D = \frac{W}{L} \mu_{eff} C_{ox} (V_{GS} - V_{th}) V_{DS} \quad (3)$$

where  $W$  is channel width,  $L$  is channel length,  $C_{OX}$  is the gate oxide capacitance per unit area, and  $\mu_{eff}$  is effective mobility.

The transconductance is usually expressed as

$$g_m = \frac{W}{L} \mu_{eff} C_{ox} V_{DS} \quad (4)$$

Thus, known as the field effect mobility

$$\mu_{FE} = \frac{L g_m}{W C_{ox} V_{DS}} \quad (5)$$

#### 4. Conclusions

We investigated the structural, morphological, and electrical characteristics of ZnO films, coating various solution concentrations at room temperature, and monitoring their performance as active channels in TFT devices. We demonstrated that the characteristic of TFT is the most stable for the ZnO solution concentration of 0.05 M. When the concentration of the ZnO solution is 0.05 M, the operation current level of a ZnO TFT is increased and the  $I_{on}/I_{off}$  ratio is improved substantially. Under these conditions, the on-off current ratio is above  $10^6$ , the channel mobility is  $0.12 \text{ cm}^2/V\cdot s$ , and the threshold current is 11.4 V. The average optical transmission of the ZnO film in the visible spectrum range is approximately 86%, and the transmission at 550 nm is 89%.

#### Acknowledgments

This work was supported by the National Science Council, Taiwan, under Contract Nos. MOST 103 – 2221 – E – 167 - 035.

## Reference

- Ameer, M.A., Ghoneim, A.A., & Fekry, A.M. (2012). Electrochemical corrosion inhibition of Al-Si alloy in phosphoric acid. *International Journal of Electrochemical Science*, 7, 4418-4431.
- Anand, V.K., Sood, S.C., & Sharma, A. (2010). Characterization of ZnO Thin Film Deposited by Sol-Gel Process. In *International Conference on Methods and Models in Science and Technology (ICM2ST-10)* (Vol. 1324, pp. 399-401). AIP Publishing.
- Bahadur, H., Srivastava, A.K., Haranath, D., Chander, H., Basu, A., Samanta, S.B., ... & Chandra, S. (2007). Nano-structured ZnO films by sol-gel process. *Indian Journal of Pure & Applied Physics*, 45, 395-399.
- Bari, A.R., Shinde, M.D., Deo, V., & Patil, L.A. (2009). Effect of solvents on the particle morphology of nanostructured ZnO. *Indian Journal of Pure & Applied Physics*, 47, 24-27.
- Bermúdez-Reyes, B., Puente-Ornelas, R., García-Pérez, U.M., Zambrano-Robledo, P., Contreras-García, M.E., Morales-Hernández, J., & Espinoza-Beltrán, F.J. (2012). Cyclic polarization and immersion corrosion test on HA/ZrO<sub>2</sub>/316LSS for application on orthopedics prosthesis. *International Journal of Electrochemical Science* 7, 2028-2035.
- Chang, Y.J., Lee, D.H., Herman, G.S., & Chang, C.H. (2007). High-performance, spin-coated zinc tin oxide thin-film transistors. *Electrochemical and solid-state letters*, 10, H135-H138.
- Cheng, H.C., Chen, C.F., & Tsay, C.Y. (2007). Transparent ZnO thin film transistor fabricated by sol-gel and chemical bath deposition combination method. *Applied physics letters*, 90, 012113.
- Cheng, H.C., Yang, P.Y., Wang, J.L., Agarwal, S., Tsai, W.C., Wang, S.J., & Lee, I.C. (2011). Zinc oxide thin-film transistors with location-controlled crystal grains fabricated by low-temperature hydrothermal method. *IEEE Electron Device Letters*, IEEE, 32, 497-499.
- Cho, K.H., Kang, M.G., Oh, S.M., Kang, C.Y., Lee, Y., & Yoon, S.J. (2010). Low voltage ZnO thin-film transistors with Ti-substituted BZN gate insulator for flexible electronics. *Thin Solid Films*, 518, 6277-6279.
- Chu, M.C., You, H.C., Meena, J.S., Shieh, S.H., Shao, C.Y., Chang, F.C., & Ko, F.H. (2012). Facile electroless deposition of zinc oxide ultrathin film for zinc acetate solution-processed transistors. *International Journal of Electrochemical Science*, 7, 5977-5989.
- Gayen, R.N., Sarkar, K., Hussain, S., Bhar, R., & Pal, A.K. (2011). ZnO films prepared by modified sol-gel technique. *Indian Journal of Pure & Applied Physics*, 49, 470-477.
- Grundmann, M., Frenzel, H., Lajn, A., Lorenz, M., Schein, F., & von Wenckstern, H. (2010). Transparent semiconducting oxides: materials and devices. *Physica status solidi (a)*, 207, 1437-1449.
- Hirao, T., Furuta, M., Hiramatsu, T., Matsuda, T., Li, C., Furuta, H., ... & Kakegawa, M. (2008). Bottom-gate zinc oxide thin-film transistors (ZnO TFTs) for AM-LCDs. *IEEE Transactions on Electron Devices*, 55, 3136-3142.
- Hoffman, R.L., Norris, B.J., & Wager, J.F. (2003). ZnO-based transparent thin-film transistors. *Applied Physics Letters*, 82, 733-735.
- Kim, D., Jeong, Y., Song, K., Park, S.K., Cao, G., & Moon, J. (2009). Inkjet-printed zinc tin oxide thin-film transistor. *Langmuir*, 25, 11149-11154.
- Lee, C., Lim, K., & Song, J. (1996). Highly textured ZnO thin films doped with indium prepared by the pyrosol method. *Solar energy materials and solar cells*, 43, 37-45.
- Lee, J.H., Ko, K.H., & Park, B.O. (2003). Electrical and optical properties of ZnO transparent conducting films by the sol-gel method. *Journal of Crystal Growth*, 247, 119-125.
- Lee, C.Y., Lin, M.Y., Wu, W.H., Wang, J.Y., Chou, Y., Su, W.F., & Lin, C.F. (2010). Flexible ZnO transparent thin-film transistors by a solution-based process at various solution concentrations. *Semiconductor Science and Technology*, 25, 105008.
- Lim, S.J., Kwon, S., & Kim, H. (2008). ZnO thin films prepared by atomic layer deposition and rf sputtering as an active layer for thin film transistor. *Thin Solid Films*, 516, 1523-1528.
- Muthukumar, S., Gorla, C.R., Emanetoglu, N.W., Liang, S., & Lu, Y. (2001). Control of morphology and orientation of ZnO thin films grown on SiO<sub>2</sub>/Si substrates. *Journal of Crystal Growth*, 225, 197-201.
- Park, S.Y., Kim, B.J., Kim, K., Kang, M.S., Lim, K.H., Lee, T.I., ... & Kim, Y.S. (2012). Low-temperature, solution-processed and alkali metal doped ZnO for high-performance thin-film transistors. *Advanced Materials*, 24, 834-838.
- Pearton, S.J., Norton, D.P., Ip, K., Heo, Y.W., & Steiner, T. (2005). Recent progress in processing and properties of ZnO. *Progress in materials science*, 50, 293-340.
- Rendón, G., Poot, P., Oliva, A.I., & Espinosa-Faller, F.J. (2012). A simple substrate heater device with temperature controller for thin film preparation. *Journal of Applied Research and Technology*, 10, 549-556.
- Spear, W.E., & Le Comber, P.G. (1993). Substitutional doping of amorphous silicon. *Solid State Communications*, 88, 1015-1018.
- Srinivasan, G., Gopalakrishnan, N., Yu, Y.S., Kesavamoorthy, R., & Kumar, J. (2008). Influence of post-deposition annealing on the structural and optical properties of ZnO thin films prepared by sol-gel and spin-coating method. *Superlattices and Microstructures*, 43, 112-119.
- Tsay, C.Y., Fan, K.S., Chen, S.H., & Tsai, C.H. (2010). Preparation and characterization of ZnO transparent semiconductor thin films by sol-gel method. *Journal of Alloys and Compounds*, 495, 126-130.
- Vázquez-Cerón, E.R., Barrales-Guadarrama, V.R., Rodríguez-Rodríguez, E.M., & Barrales-Guadarrama, R. (2007). Principal factors determination in the growth of thin films using Taguchi's technique. *Journal of Applied Research and Technology*, 5, 113-120.
- Wu, M.S., Shih, W.C., & Tsai, W.H. (1998). Growth of ZnO thin films on interdigital transducer/Corning 7059 glass substrates by two-step fabrication methods for surface acoustic wave applications. *Journal of Physics D: Applied Physics*, 31, 943.
- You, H.C., & Lin, Y.H. (2012). Investigation of the sol-gel method on the flexible ZnO device. *International Journal of Electrochemical Science* 7, 9085-9094.